

ON THE COMPUTATION OF THE EXACT OVERALL CONSISTENT TANGENT MODULI FOR NON-LINEAR FINITE STRAIN HOMOGENIZATION PROBLEMS USING SIX FINITE PERTURBATIONS

J. Kochmann¹, T. Brepols¹, S. Wulfinghoff¹, B. Svendsen^{2,3} and S. Reese¹

¹ Institute of Applied Mechanics, RWTH Aachen University, D-52074 Aachen, Germany,
{julian.kochmann, tim.brepols, stephan.wulfinghoff, stefanie.reese}@rwth-aachen.de

² Material Mechanics, RWTH Aachen University, Schinkelstr. 2, D-52062 Aachen, Germany

³ Microstructure Physics and Alloy Design, Max-Planck-Institut für Eisenforschung GmbH,
D-40237 Düsseldorf, Germany, b.svendsen@mpie.de

Key words: Two-scale, FE-FFT, Crystal plasticity, Polycrystals, Overall algorithmic tangent

Abstract. This work is concerned with the development of a numerically robust two-scale computational approach for the prediction of the local and overall mechanical behavior of heterogeneous materials with non-linear constitutive behavior at finite strains. Assuming scale separation, the macroscopic constitutive behavior is determined by the mean response of the underlying microstructure which is attached to each macroscopic integration point in the form of a periodic unit cell. The algorithmic formulation and numerical solution of the two locally-coupled boundary value problems is based on the FE-FFT method (e.g. [14, 17]). In particular, a numerically robust algorithmic formulation for the computation of the overall consistent algorithmic tangent moduli is presented. The underlying concept is a perturbation method. In contrast to existing numerical tangent computation algorithms the proposed method yields the exact tangent using only six (instead of nine) perturbations (3 in 2d). As an example, the micromechanical fields and effective material behavior of elasto-viscoplastic polycrystals are predicted for representative simulation examples.

1 INTRODUCTION

Most materials of technological importance (e.g. polycrystals, high-strength ceramics, fiber-reinforced composites) are characterized by complex microstructures which are governed by non-linear constitutive relations (e.g. plasticity, damage), in general. Thus, the prediction of the overall constitutive response of heterogeneous media represents a challenging task. In order to capture macroscopic boundary conditions as well as microstructural details, scale separation might be assumed and two-scale full-field models be employed. Recently, FE-FFT methods (e.g. [14, 17, 18]) have been developed which make use of a finite element (FE)-based algorithmic formulation and numerical solution of

the macroscopic boundary value problem (BVP) and fast Fourier transforms (FFT) and fixed-point methods (e.g. [5, 7]) for an iterative solution of the microscopic BVP. Since FFT-based micromechanical solvers have been shown (e.g. [11, 13]) to be more efficient than FE-based solvers in many cases, FE-FFT-based approaches seem to be a promising alternative to the classical FE² method (e.g. [8]). Using the classical Newton-Raphson scheme for the solution of the macroscopic BVP, the computation of the overall consistent tangent moduli is required for the linearization procedure. In the context of FE-FFT methods numerical tangent computations (e.g. [17, 18]) have been used in most cases for simplicity which is correlated to high computational costs, in general. Recently, [19] proposed a numerical scheme to compute the tangent directly based on the Lippmann-Schwinger [2] equation. However, such direct tangent computations might be associated with high memory allocations and less efficient for sophisticated large strain constitutive laws with anisotropy or complex microstructures.

The purpose of this paper is the derivation of a numerically robust algorithmic formulation for the numerical computation of the overall consistent algorithmic tangent moduli. The proposed perturbation-based algorithm ensures quadratic convergence for finite perturbations using a small number of stress computations. As an example, the FE-FFT method (e.g. [17, 18]) is employed to predict the local and effective mechanical behavior of polycrystalline aggregates with elasto-viscoplastic constitutive behavior at finite strains.

This paper is structured as follows: The two-scale problem and micro-to-macro transition is reviewed in Section 2. In Section 3 the phenomenological finite strain crystal plasticity constitutive model for single crystal grains is presented in a nutshell. The microscopic FFT- and macroscopic FE-based algorithmic formulation is introduced in Section 4. Basic numerical results and representative simulation examples are presented in Section 5. The paper ends with a summary and discussion in Section 6.

2 TWO-SCALE BOUNDARY VALUE PROBLEM

If not stated otherwise, all differential operators are defined in and referred to the reference configuration.

2.1 MACROSCOPIC PROBLEM

Let us consider the macroscopic structure $\overline{\Omega}$ with boundary $\partial\overline{\Omega}$ on which displacement and/or traction boundary conditions are applied. The deformation at point $\overline{\mathbf{X}} \in \overline{\Omega}$ is described by the displacement vector $\overline{\mathbf{u}}$ from which the macroscopic deformation gradient $\overline{\mathbf{F}}(\overline{\mathbf{X}}) = \mathbf{I} + \text{Grad } \overline{\mathbf{u}}(\overline{\mathbf{X}})$ is deduced. Conservation of quasi-static linear momentum in the absence of body forces requires

$$\text{Div } \overline{\mathbf{P}}(\overline{\mathbf{X}}) = \mathbf{0} \quad \text{in } \overline{\Omega} \quad (1)$$

where $\overline{\mathbf{P}}(\overline{\mathbf{X}}) = \overline{\mathbf{P}}(\overline{\mathbf{X}}, \overline{\mathbf{F}})$ denotes the macroscopic first Piola-Kirchhoff stress tensor.

2.2 MICROSCOPIC PROBLEM

The overall constitutive relation $\overline{\mathbf{P}}(\overline{\mathbf{X}})$ is defined by the mean response of the underlying microstructure which is attached to each $\overline{\mathbf{X}} \in \overline{\Omega}$ in the form of a periodic unit cell (UC) of the domain Ω . Microstructural deformations are assumed to be dictated by $\overline{\mathbf{F}}$. Thus, we may assume the deformation gradient \mathbf{F} to be additively split into the imposed macroscopic deformation gradient $\overline{\mathbf{F}}$ and a spatially heterogeneous fluctuation field $\tilde{\mathbf{H}}$ such that

$$\mathbf{F}(\mathbf{X}; \overline{\mathbf{X}}) = \overline{\mathbf{F}}(\overline{\mathbf{X}}) + \tilde{\mathbf{H}}(\mathbf{X}) \quad (2)$$

where $\tilde{\mathbf{H}}(\mathbf{X}) = \text{Grad } \tilde{\mathbf{u}}(\mathbf{X})$ denotes the fluctuation field of the local displacement gradient. Let us establish the microscopic constitutive relation $\mathbf{P}(\mathbf{X}) = \mathbf{P}(\mathbf{X}, \mathbf{F}, \dot{\mathbf{F}}, \boldsymbol{\chi})$ at each $\mathbf{X} \in \Omega$ for an arbitrary rate-dependent material with internal variables $\boldsymbol{\chi}$ to define the microscopic BVP for quasi-static mechanical equilibrium

$$\text{Div } \mathbf{P}(\mathbf{X}) = \mathbf{0} \quad \text{in } \Omega \quad (3)$$

in analogy to (1). Periodic micromechanical fields are assumed which implies periodic deformations and antiperiodic tractions.

2.3 SCALE TRANSITION

The macroscopic deformation gradient $\overline{\mathbf{F}}$ and its work-conjugate stress measure $\overline{\mathbf{P}}$

$$\overline{\mathbf{F}} = \frac{1}{V} \int_{\Omega} \mathbf{F} dV \quad \text{and} \quad \overline{\mathbf{P}} = \frac{1}{V} \int_{\Omega} \mathbf{P} dV \quad (4)$$

are defined through the volume averages of their local fields \mathbf{F} and \mathbf{P} with $V = \text{vol}(\Omega)$. Thus, the handshake between both scales only requires the transfer of $\overline{\mathbf{F}}$ and $\overline{\mathbf{P}}$, respectively.

3 CONSTITUTIVE MODEL

The constitutive model formulation used in this work is based on earlier work by [1, 4] and others. We assume the deformation gradient

$$\mathbf{F} = \mathbf{F}_e \mathbf{F}_p \quad (5)$$

to be multiplicatively decomposed into elastic \mathbf{F}_e and plastic \mathbf{F}_p parts. The superposition of the contribution of multiple slip systems $\alpha = 1, \dots, n_{\text{slip}}$ defines the plastic velocity gradient

$$\mathbf{L}_p = \sum_{\alpha=1}^{n_{\text{slip}}} \dot{\gamma}_{\alpha} \mathbf{d}_{\alpha} \otimes \mathbf{n}_{\alpha} = \dot{\mathbf{F}}_p \mathbf{F}_p^{-1} \quad (6)$$

where \mathbf{d}_{α} and \mathbf{n}_{α} represent the slip direction and plane normal. The second Piola-Kirchhoff stress $\mathbf{S}_e = \mathbb{C} : \mathbf{E}_e$ is introduced in terms of the elastic stiffness \mathbb{C} and Green-Lagrange strain $\mathbf{E}_e = \frac{1}{2}(\mathbf{F}_e^{\top} \mathbf{F}_e - \mathbf{I})$ in the intermediate configuration to define the resolved shear rate as

$$\tau_{\alpha}(\mathbf{M}_e) = \mathbf{M}_e \cdot (\mathbf{d}_{\alpha} \otimes \mathbf{n}_{\alpha}) \quad (7)$$

where $\mathbf{M}_e = \mathbf{C}_e \mathbf{S}_e$ denotes the Mandel stress with $\mathbf{C}_e = \mathbf{F}_e^\top \mathbf{F}_e$. If (7) exceeds a critical value τ^c , the material is considered to flow yielding irreversible deformations. The critical resolved shear stress (CRSS) τ^c is related to the accumulated plastic slip $\gamma_{\text{acc}} = \sum_\alpha \int |\dot{\gamma}_\alpha| dt$ through $\tau^c(\gamma_{\text{acc}}) = \tau_0^c + q_h(\gamma_{\text{acc}})$, where τ_0^c denotes the initial CRSS and $q_h(\gamma_{\text{acc}})$ an isotropic hardening function. The powerlaw type flow rule

$$\dot{\gamma}_\alpha = \dot{\gamma}_0 \left\langle \frac{|\tau_\alpha| - \tau^c}{\tau^D} \right\rangle^p \text{sgn}(\tau_\alpha) \quad (8)$$

is defined in terms of the drag stress τ^D , rate sensitivity parameter p and reference shear rate $\dot{\gamma}_0$. Voce-type hardening behavior is assumed which is described by the hardening function

$$q_h(\gamma_{\text{acc}}) = \tau_0^c + (\tau_\infty - \tau_0) \tanh\left(\frac{(h_0 - h_\infty)\gamma_{\text{acc}}}{\tau_\infty - \tau_0^c}\right) + h_\infty \gamma_{\text{acc}} \quad (9)$$

h_0, h_∞ and τ_∞ are material parameters. The plastic deformation gradient \mathbf{F}_p and the accumulated plastic slip γ_{acc} define the set of internal variables $\boldsymbol{\chi} = \{\mathbf{F}_p^{-1}, \gamma_{\text{acc}}\}$.

The flow rule (8) is assumed to be discretized using an implicit time integration scheme (e.g. backward Euler). For moderate and high rate-sensitivity parameters p , small time increments Δt are required to ensure local convergence, in general. Following [22, 20], we may assume a continuously differentiable transition between the powerlaw and a linear approximation. The regularized solution gives an improved initial guess for the non-regularized solution which leads to local convergence for relatively large time increments Δt and high values for p . The underlying algorithm ensures that the regularized solution coincides with the original powerlaw solution at convergence. Details on the discretized set of local equilibrium equations and the implementation of the solution algorithm for finite strain elasto-viscoplasticity which is used in this work can be found in [20] and [21].

4 ALGORITHMIC FORMULATIONS

The algorithmic formulation and numerical solution scheme of the two locally-coupled BVPs (1) and (3) is based on the FE-FFT method (e.g. [14, 17]) and explained in a nutshell, in what follows.

4.1 FINITE ELEMENT DISCRETIZATION OF MACROSCOPIC EQUATIONS

The weak form of the macroscopic balance of linear momentum

$$\bar{g}(\bar{\mathbf{u}}, \delta \bar{\mathbf{u}}) = \int_{\bar{\Omega}} \bar{\mathbf{S}} \cdot \delta \bar{\mathbf{E}} dV - \int_{\partial_{\bar{\mathbf{t}}}\bar{\Omega}} \bar{\mathbf{t}}_0 \cdot \delta \bar{\mathbf{u}} dA = 0 \quad \forall \delta \bar{\mathbf{u}} \quad (10)$$

is derived based on the principle of virtual work with corresponding boundary conditions $\bar{\mathbf{u}} = \bar{\mathbf{u}}_0$ on $\partial_{\bar{\mathbf{u}}}\bar{\Omega}$ and/or $\bar{\mathbf{t}} = \bar{\mathbf{t}}_0$ on $\partial_{\bar{\mathbf{t}}}\bar{\Omega}$, respectively with

$$\delta \bar{\mathbf{E}} = \frac{1}{2} \left(\bar{\mathbf{F}}^\top \text{Grad} \delta \bar{\mathbf{u}} + \text{Grad} \delta \bar{\mathbf{u}}^\top \bar{\mathbf{F}} \right) \quad (11)$$

As usual, (10) vanishes at equilibrium for arbitrary test functions $\delta\bar{\mathbf{u}}$. Any discretization $\bar{\Omega} \approx \bigcup_{e=1}^{n_{\text{elem}}} \bar{\Omega}^e$ of $\bar{\Omega}$ into n_{elem} elements and linearization of (10) with respect to $\bar{\mathbf{u}}$ induces

$$\begin{aligned} \int_{\bar{\Omega}} \text{Grad } \delta\bar{\mathbf{u}} \cdot (\text{Grad } \Delta\bar{\mathbf{u}} \bar{\mathbf{S}}) dV + \int_{\bar{\Omega}} \delta\bar{\mathbf{E}} \cdot \frac{\partial \bar{\mathbf{S}}}{\partial \bar{\mathbf{E}}} [\Delta\bar{\mathbf{E}}] dV = \\ - \int_{\bar{\Omega}} \delta\bar{\mathbf{E}} \cdot \bar{\mathbf{S}} dV + \int_{\partial_{\bar{\mathbf{t}}}\bar{\Omega}} \bar{\mathbf{t}}_0 \cdot \delta\mathbf{u} dA \quad \forall \delta\bar{\mathbf{u}} \end{aligned} \quad (12)$$

Introducing the approximations

$$\bar{\mathbf{u}} \approx \mathbf{N}_{\bar{\mathbf{u}}}^e \bar{\mathbf{u}}^e, \quad \delta\bar{\mathbf{u}} \approx \mathbf{N}_{\bar{\mathbf{u}}}^e \delta\bar{\mathbf{u}}^e, \quad \text{Grad}(\bar{\mathbf{u}}) \approx \mathbf{B}_{\bar{\mathbf{u}}}^e \bar{\mathbf{u}}^e, \quad \text{Grad}(\delta\bar{\mathbf{u}}) \approx \mathbf{B}_{\bar{\mathbf{u}}}^e \delta\bar{\mathbf{u}}^e \quad (13)$$

and

$$\mathbf{B}_{\bar{\mathbf{u}}}^e = \text{Grad}(\mathbf{N}_{\bar{\mathbf{u}}}^e), \quad \Delta\bar{\mathbf{E}} \approx \mathbf{G}_{\bar{\mathbf{u}}}^e \Delta\bar{\mathbf{u}}^e, \quad \delta\bar{\mathbf{E}} \approx \mathbf{G}_{\bar{\mathbf{u}}}^e \delta\bar{\mathbf{u}}^e \quad (14)$$

leads to the following set of non-linear equations in Voigt notation (denoted by the index V)

$$\begin{aligned} \sum_{e=1}^{n_{\text{elem}}} \delta\bar{\mathbf{u}}^{e\top} \left\{ \left(\int_{\bar{\Omega}^e} \mathbf{B}_{\bar{\mathbf{u}}}^{e\top} \mathbb{D}^e \mathbf{B}_{\bar{\mathbf{u}}}^e dV + \int_{\bar{\Omega}^e} \mathbf{G}_{\bar{\mathbf{u}}}^{e\top} \left(\frac{\partial \bar{\mathbf{S}}_v}{\partial \bar{\mathbf{E}}_v} \right)^e \mathbf{G}_{\bar{\mathbf{u}}}^e dV \right) \Delta\bar{\mathbf{u}}^e \right\} = \\ - \sum_{e=1}^{n_{\text{elem}}} \delta\bar{\mathbf{u}}^{e\top} \left\{ \int_{\bar{\mathcal{B}}^e} \mathbf{G}_{\bar{\mathbf{u}}}^{e\top} \bar{\mathbf{S}}_v^e dV - \int_{\partial_{\bar{\mathbf{t}}}\bar{\Omega}^e} \mathbf{N}_{\bar{\mathbf{u}}}^{e\top} \bar{\mathbf{t}}_0 dA \right\} \end{aligned} \quad (15)$$

with $D_{ijkl}^e = S_{jl}^e \delta_{ik}$. Classical assembly of the left- and right-hand side of (15) leads to the global system of equations which is solved for the global nodal displacement increment using the Newton-Raphson scheme. Quadratic convergence is obtained by consistently linearizing (10) and computing the overall algorithmic tangent

$$\bar{\mathbf{A}}^e = \left(\frac{\partial \bar{\mathbf{S}}_v}{\partial \bar{\mathbf{E}}_v} \right)^e \quad (16)$$

4.1.1 OVERALL CONSISTENT TANGENT COMPUTATION

Different perturbation-based methods have been proposed to compute the overall consistent tangent numerically. For example, [6] developed an efficient algorithm to compute (16) based on three (2D) or six (3D) perturbations in finite strain theory. However, the convergence behavior of the FE-solver is strongly influenced by the choice of the perturbation value. In what follows, an algorithmic formulation is presented which leads to quadratic convergence based on three (2D) or six (3D) finite perturbations.

The macroscopic deformation gradient $\bar{\mathbf{F}}$ and its work-conjugate stress measure $\bar{\mathbf{P}}$ defined via (4) are related through $d\bar{\mathbf{P}} = \bar{\mathbb{G}} : d\bar{\mathbf{F}}$, where $\bar{\mathbb{G}}$ denotes the overall algorithmic tangent operator. Polar decomposition of $\bar{\mathbf{F}}$ leads to

$$d\bar{\mathbf{P}} = \bar{\mathbb{G}} : d\bar{\mathbf{F}} = \bar{\mathbb{G}} : (\bar{\mathbf{R}}_0 \cdot d\bar{\mathbf{U}}) \quad (17)$$

assuming fixed rotations $\overline{\mathbf{R}}_0$ for each macroscopic load step. Let us formulate the overall constitutive relation in terms of $\overline{\mathbf{U}}$ and the Biot stress

$$\overline{\mathbf{T}} = \frac{1}{2} \left(\overline{\mathbf{R}}_0^\top \cdot \overline{\mathbf{P}} + \overline{\mathbf{R}}_0 \cdot \overline{\mathbf{P}}^\top \right) = \text{sym}(\overline{\mathbf{U}} \cdot \overline{\mathbf{S}}) \quad (18)$$

which allows us to construct the algorithmic tangent $\overline{\mathbb{B}} = \partial_{\overline{\mathbf{U}}} \overline{\mathbf{T}}$ based on 3 (2D) or 6 perturbations (3D). Suppose that $\overline{\mathbb{B}}$ can be computed exactly, linearization of (18) gives

$$d\overline{\mathbf{T}} \stackrel{!}{=} \overline{\mathbb{B}} : d\overline{\mathbf{U}} \quad \text{with} \quad d\overline{\mathbf{T}} = \frac{1}{2} (d\overline{\mathbf{U}} \cdot \overline{\mathbf{S}} + \overline{\mathbf{U}} \cdot d\overline{\mathbf{S}} + \overline{\mathbf{S}} \cdot d\overline{\mathbf{U}} + d\overline{\mathbf{S}} \cdot \overline{\mathbf{U}}) \quad (19)$$

Factorization of (19) with respect to $d\overline{\mathbf{T}}$ and $d\overline{\mathbf{U}}$ and rearrangement leads to

$$\underbrace{\left(\overline{\mathbf{U}} \overset{\text{sym}}{\square} \mathbf{I} + \mathbf{I} \overset{\text{sym}}{\square} \overline{\mathbf{U}} \right)}_{\mathbb{E}^{-1}} : d\overline{\mathbf{S}} = \underbrace{\left(2\overline{\mathbb{B}} - (\overline{\mathbf{S}} \overset{\text{sym}}{\square} \mathbf{I} + \mathbf{I} \overset{\text{sym}}{\square} \overline{\mathbf{S}}) \right)}_{\mathbb{D}} : d\overline{\mathbf{U}} \quad (20)$$

where the short-hand notation

$$\left(\mathbf{Q} \overset{\text{sym}}{\square} \mathbf{I} \right)_{ijkl} = \frac{1}{2} (Q_{ik}\delta_{jl} + Q_{il}\delta_{jk} + Q_{lj}\delta_{ik} + Q_{kj}\delta_{il}) \quad (21)$$

was introduced for convenience. Since $d\overline{\mathbf{S}} = (\mathbb{E} : \mathbb{D}) : d\overline{\mathbf{U}}$ and $d\overline{\mathbf{C}} = \mathbb{E}^{-1} : d\overline{\mathbf{U}}$, (20) can be reformulated as

$$d\overline{\mathbf{S}} = \underbrace{2(\mathbb{E} : \mathbb{D} : \mathbb{E})}_{\overline{\mathbb{A}}} : d\overline{\mathbf{E}} \quad (22)$$

which represents the constitutive relation between $\overline{\mathbf{S}}$ and $\overline{\mathbf{E}}$. Replacing the local constitutive form by its linearized version

$$\mathbf{P}^{(i+1)} = \mathbf{P}^{(i)} + \partial_{\mathbf{F}} \mathbf{P}|_{\mathbf{F}^{(i)}} : (\mathbf{F}^{(i+1)} - \mathbf{F}^{(i)}) \quad (23)$$

for the numerical tangent computation, the overall constitutive relation $\overline{\mathbf{T}}(\overline{\mathbf{U}})$ is linearly dependent on $\overline{\mathbf{U}}$ via (17). Since the local fields $\mathbf{F}^{(i)}$, $\mathbf{P}^{(i)}$ and $\partial_{\mathbf{F}} \mathbf{P}|_{\mathbf{F}^{(i)}}$ are known from the stress computation, only a system of linear equations has to be solved for each perturbation in $\overline{\mathbf{U}}$ at the micro scale. As a result, quadratic convergence is observed at the FE-level using three (2D) or six (3D) finite perturbations.

4.2 LIPPMANN-SCHWINGER EQUATION FOR FINITE STRAINS

Based on the pioneering work for linearized kinematics by [2, 3] and recent FFT-based iterative solution methods for the geometrically non-linear theory [10, 13], the constitutive relation is reformulated based on a polarization field

$$\boldsymbol{\tau}(\mathbf{F}) = \mathbf{P} - \mathbb{C}^{(0)} : \mathbf{F} \quad (24)$$

which defines the difference in material properties between the microstructure and a homogeneous reference material with elastic stiffness $\mathbb{C}^{(0)}$. Making use of Green's function $\mathbf{G}^{(0)}$ associated with $\mathbb{C}^{(0)}$ solves the reformulated local problem

$$\text{Div}(\mathbb{C}^{(0)} : \mathbf{F}) = -\text{Div}(\boldsymbol{\tau}) \quad \text{in } \Omega \quad (25)$$

yielding the Lippmann-Schwinger equation (e.g. [2])

$$\mathbf{F} = \overline{\mathbf{F}} - \mathbb{F}^{(0)} * \boldsymbol{\tau} \quad \text{in } \Omega \quad (26)$$

where

$$(\mathbb{F}^{(0)} * \boldsymbol{\tau})(\mathbf{X}) = \int_{\Omega} \mathbb{F}^{(0)}(\mathbf{X}, \mathbf{Y}) : \boldsymbol{\tau}(\mathbf{Y}) \, d\mathbf{Y} \quad (27)$$

denotes the convolution integral between the Green's operator $\mathbb{F}^{(0)}$ and $\boldsymbol{\tau}$. The integral equation (26) can efficiently be solved using FFT- and fixed-point methods (e.g. [5, 7, 13]). Assuming an isotropic reference material with elastic constants $\mu^{(0)}$ and $\lambda^{(0)}$, closed-form expressions for the Green's function tensor $\hat{\mathbf{G}}^{(0)}$ and its kernel $\hat{\mathbb{F}}^{(0)}$

$$\left(\hat{G}_{ik}^{(0)}(\boldsymbol{\xi})\right)^{-1} = C_{ijkl}^{(0)} \xi_j \xi_l, \quad \hat{I}_{ijkl}^{(0)}(\boldsymbol{\xi}) = \hat{G}_{ik}^{(0)}(\boldsymbol{\xi}) \xi_j \xi_l \quad \text{for } \boldsymbol{\xi} \neq \mathbf{0} \quad (28)$$

are available in Fourier space. Note that the short-hand notation $\hat{\mathbf{f}}(\boldsymbol{\xi}) = \text{FFT}\{\mathbf{f}(\mathbf{X})\}$ was introduced for convenience, where $\boldsymbol{\xi}$ denotes the frequency vector. Solving the linearized Lippmann-Schwinger equation

$$\Delta \mathbf{F}^{(i+1)} + \mathbb{F}^{(0)} * [(\partial_{\mathbf{F}} \mathbf{P}|_{\mathbf{F}^{(i)}} - \mathbb{C}^{(0)}) : \Delta \mathbf{F}^{(i+1)}] = \overline{\mathbf{F}} - \mathbb{F}^{(0)} * \mathbf{P}^{(i)}(\mathbf{F}^{(i)}) \quad (29)$$

for $\Delta \mathbf{F}^{(i+1)}$ by means of FFT- and Newton-Krylov subspace methods (e.g. conjugate gradients [15], GMRES [16]) leads to quadratic convergence independent of the choice of $\mathbb{C}^{(0)}$ as shown by [12].

In this work a FFT- and conjugate gradient-based micromechanical solver with the convergence criterion $\|\Delta \mathbf{F}^{(i+1)}\| / \|\overline{\mathbf{F}}\| < \text{tol}_{\Delta \mathbf{F}}$ is implemented. An improved starting solution for the micromechanical fields $\mathbf{F}^{(i)}$, $\mathbf{P}^{(i)}$ and $\partial_{\mathbf{F}} \mathbf{P}|_{\mathbf{F}^{(i)}}$ is obtained by performing a few fixed-point iterations before each Newton step. Details can be found in [18].

5 NUMERICAL EXAMPLE

For simplicity attention is restricted to two-dimensional numerical examples assuming a plane strain condition. A polycrystalline microstructure consisting of 100 randomly distributed grains with random orientations is sampled on a square unit cell. The latter is embedded in each integration point of the macroscopic structure. In order to increase the efficiency of the proposed two-scale approach, a reduced integration-based FE formulation with hourglass stabilization is used yielding one integration point per element (e.g. [9]). The material parameters used for the micromechanical crystal plasticity model are summarized in Table 1. The FFTW-library (www.fftw.org) is employed for the (inverse) Fourier transform of any local field. The two-scale model is implemented as a user element into the finite element software feap (www.ce.berkeley.edu/projects/feap/).

C_{11} [GPa]	C_{12} [GPa]	C_{44} [GPa]	τ_0^c [MPa]	τ^D [MPa]	τ_∞ [MPa]	h_0 [MPa]	p [-]
236	134	119	1	150	420	500.0	20

Table 1: Used material parameters. Furthermore, $\dot{\gamma}_0 = 1/s$ was set.

Since the focus of this paper is the convergence of the macroscopic FE-solver, the discretization of the microstructural domain is rather coarse. $N = 63$ grid points are used for the discretization in each spatial direction. The polygrain microstructure is visualized in the right part of Figure 1. In the left part of Figure 1 the macroscopic structure with boundary conditions is shown. The left side of the structure $\bar{\Omega}$ is clamped and the right edge is subjected to a force $\bar{f}_2 = 100$ N in x_2 -direction applied in 150 loadsteps. This example is known as Cook’s membrane. In what follows, the numerical tangent

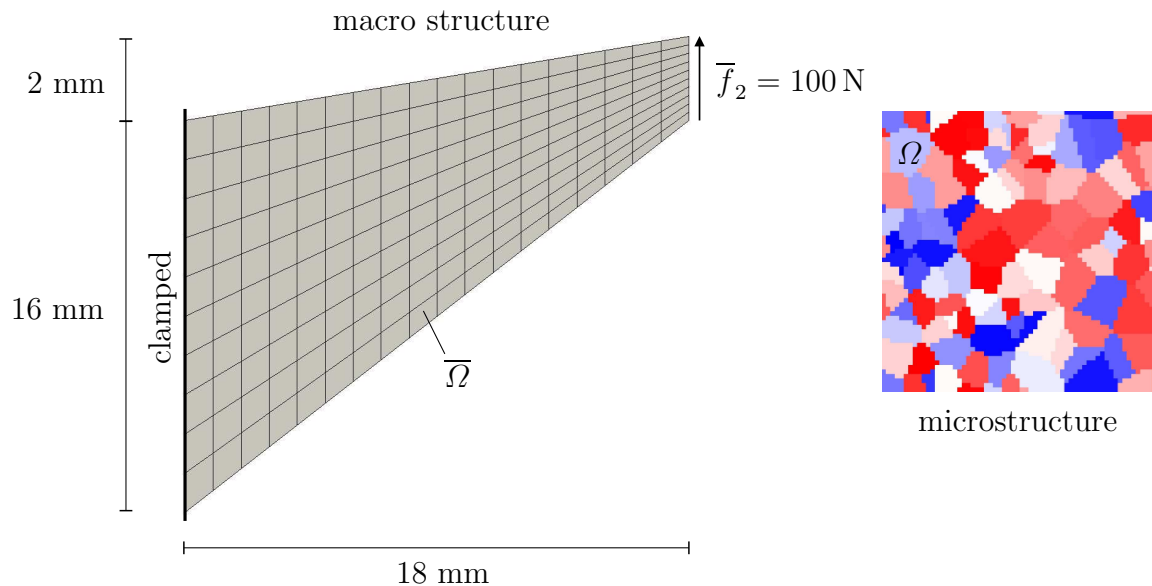


Figure 1: FE-discretized macro structure with boundary conditions (left) and Fourier-discretized microstructure (right). The latter is embedded in each macroscopic integration point.

computation method proposed by [6] is denoted as "method 1" and the new model which was introduced in Section 4.1.1 by "new method". Both methods are used to compute the overall consistent tangent moduli for the two-scale numerical example schematically drawn in Figure 1 based on different values for the underlying perturbation value ζ .

perturbation ζ	10^{-07}	10^{-05}	10^{-03}	10^{-01}	10^{+01}	10^{+03}	10^{+05}	10^{+07}
new method	4.7	4.7	4.7	4.7	4.7	4.7	4.7	4.7
method 1	4.7	5.74	7.28	x	x	x	x	x

Table 2: Average number of macroscopic iterations per macroscopic loadstep of two-scale simulation described by Figure 1 for different perturbation values of ζ . Divergence of the macroscopic FE-solver is denoted by "x".

In Table 2 the average number of macroscopic Newton iterations per load step is summarized. The results show that the "new method" is characterized by the same number of iterations independent of ζ . For "method 1" the number of Newton iterations increases with increasing ζ and breaks down for $\zeta > 10^{-3}$. Note that simulations were also conducted based on $\zeta = 10^{-08}$ and $\zeta = 10^{-09}$. The average number of FE iterations for "method 1" was not smaller than 4.7 in both cases. For any investigated value of ζ the convergence rate for the "new method" is quadratic. As an example, the convergence rate of the last macroscopic load step is visualized in Table 3 using the "new method".

iteration	residual
1	$6.13962 \cdot 10^{+01}$
2	$4.56745 \cdot 10^{+01}$
3	$3.62998 \cdot 10^{+00}$
4	$4.30757 \cdot 10^{-02}$
5	$2.29316 \cdot 10^{-05}$
6	$6.13503 \cdot 10^{-09}$

Table 3: Convergence rate of macroscopic FE-solver for the last macroscopic load step with $\zeta = 10^{+03}$ using the "new method".

For completeness, the accumulated plastic slip is visualized for one selected element in the right part of Figure 2. In the left part of Figure 2 the first component of the macroscopic first Piola-Kirchhoff stress tensor is shown. Both figures correspond to the last converged load step.

6 CONCLUSION

In this paper a numerically robust algorithmic formulation for the computation of the overall consistent algorithmic tangent moduli of non-linear heterogeneous materials in a finite strain framework was derived. The underlying concept is based on a perturbation technique and linearized local constitutive form. The special structure of the developed

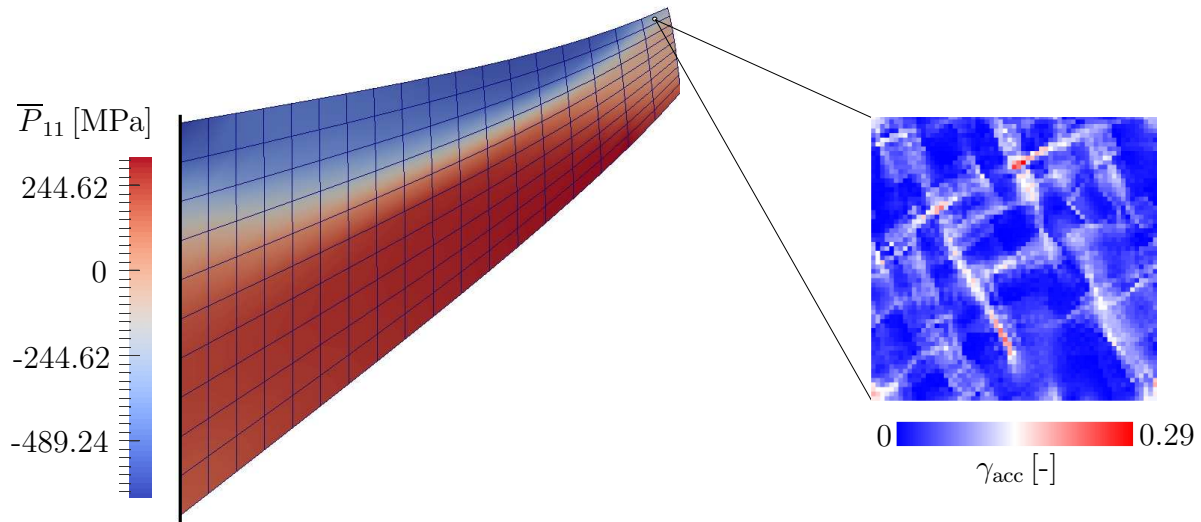


Figure 2: Visualization of macroscopic stress component \bar{P}_{11} and local accumulated plastic slip γ_{acc} for the last converged load step.

tangent computation algorithm leads to quadratic convergence for finite perturbations using three (2D) or six (3D) stress computations. Thus, the proposed scheme represents a good compromise between numerical robustness and low memory allocation. However, further simulation examples have to be conducted and different BVPs to be analyzed in order to verify the observations that have been made in this paper.

Acknowledgements: Financial support of Subproject M03 of the Transregional Collaborative Research Center SFB/TRR 136 by the German Science Foundation (DFG) is gratefully acknowledged.

REFERENCES

- [1] Lee, E. H. Elastic-plastic deformation at finite strains. *J. Appl. Mech.* (1969) **36** (1):1–6.
- [2] Kröner, E. *Statistical Continuum Mechanics*. Springer-Verlag, CISM Lecture Notes **92**, 1972.
- [3] Willis, J. R. Variational and related methods for the overall properties of composites. *In: C. S. Yih, Ed. Advances in Applied Mechanics*. (1981) **21**.
- [4] Asaro, R. J. Crystal Plasticity. *J. Appl. Mech.* (1983) **50**:921–934.
- [5] Moulinec, H. and Suquet, P. A fast numerical method for computing the linear and nonlinear mechanical properties of composites. *Comput. Method. Appl. M.* (1994) **318**:1417–1423.
- [6] Miehe, C. Numerical computation of algorithmic (consistent) tangent moduli in large-strain computational inelasticity. *Comput. Method. Appl. M.* (1996) **134**:223–240.

- [7] Moulinec, H. and Suquet, P. A numerical method for computing the overall response of nonlinear composites with complex microstructures. *Comput. Method. Appl. M.* (1998) **157** (1):69–94.
- [8] Feyel, F. and Chaboche, J. L. FE² multiscale approach for modeling the elastoviscoplastic behaviour of long fibre SiC/Ti composite materials. *Comput. Method. Appl. M.* (2000) **183**:309–330.
- [9] Reese, S. On the equivalence of mixed element formulations and the concept of reduced integration in large deformation problems. *Int. J. Numer. Meth. Eng.* (2002) **3**:1–33.
- [10] Lahellec, N. and Michel, J. C. and Moulinec, H. and Suquet, P. Analysis of inhomogeneous materials at large strains using fast Fourier transforms. *IUTAM Symposium on computational mechanics of solid materials at large strains, Solid mechanics and its applications* (2003) **108**:247–258.
- [11] Liu, B. and Raabe, D. and Roters, F. and Eisenlohr, P. and Lebensohn, R. Comparison of finite element and fast Fourier transform crystal plasticity solvers for texture prediction. *Model. Simul. Mater. Sc.* (2010) **18**.
- [12] Zeman, J. and Vodrejc, J. and Novak, J. and Marek, J. Accelerating a FFT-based solver for numerical homogenization of a periodic media by conjugate gradients. *J. Comput. Phys.* (2010) **229** (21):8065–8071.
- [13] Eisenlohr, P. and Diehl, M. and Lebensohn, R. A. and Roters, F. A spectral method solution to crystal elasto viscoplasticity at finite strains. *Int. J. Plasticity* (2013) **46**:37–53.
- [14] Spahn, J. and Andrae, H. and Kabel, M. and Müller, R. A multiscale approach for modeling progressive damage of composite materials using fast Fourier transforms. *Comput. Method. Appl. M.* (2014) **268**:871–883.
- [15] Kabel, M. and Böhlke, T. and Schneider, M. Efficient fixed point and Newton-Krylov solvers for FFT-based homogenization of elasticity at large deformations. *Comput. Mech.* (2014) **54**:1497–1514.
- [16] Shanthraj, P. and Eisenlohr, P. and Diehl, M. and Roters, F. Numerically robust spectral methods for crystal plasticity simulations of heterogeneous materials. *Int. J. Plasticity* (2015) **66**:31–45.
- [17] Kochmann, J. Mianroodi, J. R. and Wulfinghoff, S. and Svendsen, B. and Reese, S. Two-scale, FE-FFT- and phase-field based computational modeling of bulk microstructure evolution and macroscopic material behavior. *Comput. Method. Appl. M.* (2016) **305**:89–110.

- [18] Kochmann, J. and Ehle, L. and Aretz, A. and Wulfinghoff, S. and Mayer, J. and Svendsen, B. and Reese, S. Efficient and accurate two-scale FE-FFT-based prediction of the effective material behavior of viscoplastic polycrystals. *Comput. Mech.* (2017) DOI: 10.1007/s00466-017-1476-2.
- [19] Göküzüm, F. and Keip, M. A. An algorithmically consistent macroscopic tangent operator for FFT-based computational homogenization. *Int. J. Numer. Meth. Eng.* (2017) **113** (4):581–600.
- [20] Alipour, A. and Wulfinghoff, S. and Bayat, H. R. and Reese, S. and Svendsen, B. The concept of control points in hybrid discontinuous Galerkin methodsApplication to geometrically nonlinear crystal plasticity. *Int. J. Numer. Meth. Eng.* (2018) DOI: 10.1002/nme.5754.
- [21] Kochmann, J. and Brepols, T. and Wulfinghoff, S. and Svendsen, B. and Reese, S. Numerically robust two-scale FE-FFT-based finite strain crystal plasticity simulations of polycrystalline materials. *In preparation* (2018).
- [22] Wulfinghoff, S. and Böhlke, T. Equivalent plastic strain gradient crystal plasticity - enhanced power law subroutine. *GAMM-Mitteilungen* (2013) **36**(2):134–148.